SIMULATION AND STUDY OF CENTRIFUGAL PUMP COMPUTATION ACCURACY BASED ON MRS AND SMM MODELS

Jiang Xin[1,2*], Zhang Lei[1]

ABSTRACT: In the CFD-based flow field simulation computation, the accuracy of the calculation model has a decisive effect on the flow field simulation. It is found that in the simulation of the internal flow field of a centrifugal pump, different models selected for the rotating area lead to different computation results under each working condition and sometimes lead to wrong ones. Based on the Multiple Reference Frame Model (MRF) and Sliding Mesh Model (SMM), this paper carries out simulation computation of the internal flow field of a vehicle cooling centrifugal pump and obtains the external behaviors and then analyze the computation process by comparing them with the test results. It is found that in the case where the MRF model is selected for the computation of the rotating area, when the centrifugal pump speed is higher than 2000rpm, the computed results are consistent with the test ones, proving the computation process is correct, but that when the rotating speed is no higher than 2000rpm, the computed result of lift is less than the test result by 18.9%, indicating that the computed result has no research value. That is because, when the rotating speed of the pump is low, the flow on the interface between the rotating and the stationary areas of the pump varies over time, which does not meet the prerequisite for the MRF model. Later, this paper selects the SMM model for the computation of the rotating area, and carries out the simulation computation under the working conditions of 1500rpm and 100L/min. According to the calculation results, the lift after one work cycle of the impeller, the lift is up to 4.8m. Through comparison with the test result, it is found the computation error is 4.4%, proving that the computed result is valid.
KEY WORDS: Computation accuracy; Multiple Reference Frame; sliding mesh; external behaviors

1 INTRODUCTION

Centrifugal pumps are widely used and have a very important place in the national economy and different industrial sectors. The traditional testing method must be used in a test only after the pump model is completed, making it very costly and time-consuming. The numerical simulation method allows the designer to simulate a flow field to study the internal flow field behaviors and external behaviors after designing the pump model, and at the same time, the pump behavior results simulated can also be used as the criteria to test the pump design so as to continuously optimize and improve the pump model. This greatly reduces the design cost and period of a pump product. The analysis of the internal flow field behaviors of the centrifugal pump is a very complicated process, so it is usually studied through both numerical simulation and experiment.

Researchers at home and abroad have carried out a lot of studies on the numerical simulation of centrifugal pumps. (Grapsas et al., 2010) obtained the external characteristic curves of the centrifugal pump under full operating conditions and at different rotating speeds through numerical simulation and experiments. In order to study the applicability of three different turbulence models in numerical simulation, (Jafarzadeh et al., 2011) took the centrifugal pump with a low specific velocity as the research subject, and selected different turbulence models in the numerical simulation to predict the external characteristics. (Jiang X et al., 2017) studied the effects of rotation on the flow field simulation, and obtained the external characteristic curves of the centrifugal pump under different working conditions through simulation and test. (Zhang M. Li S., 2013) studied the hydrodynamic performance of the propeller by using the sliding mesh technology, and used a single processor to carry out parallel computation of the unsteady hydrodynamic performance of the propeller, the result of which was closer to the experimental value compared with that provided by the steady-state computation. (He Z H et al., 2015) analyzed the effects of the full-flow-field meshing method on the numerical prediction accuracy of the centrifugal pump from the topological relation of the computational domain and the processing method for the static and dynamic interface. Computational fluid dynamics (CFD) provides an effective way to study the internal flow fields and structural design of centrifugal pumps, which greatly improves the research efficiency. However, the computational models selected and applied have

1 College of Mechanical Science and Engineering, Jilin University, Changchun City, 130025, China
2 College of Civil Engineering, Jilin Jianzhu University, Changchun City, 130118, China
E-mail: 660-jx@163.com

great impacts on the computation accuracy, and sometimes lead to inaccurate computation results.

This paper calculates the internal flow field of an automobile engine cooling pump, uses the FLUENT software selects the standard κ-ω turbulence model and the standard wall equation, and selects the Multiple Reference Frame model (MRF) and the Sliding Mesh model (SMM) for the rotating area to study the characteristic curves of the centrifugal pumps of the same type at different speeds and analyzes them by comparing them with the test results.

2 EXAMPLE DESIGN

2.1 Turbulence model

For the flow field calculation, the *k-ω* SST turbulence model is adopted, which is defined using the following formulas:

$$\rho\frac{\partial k}{\partial t}+\rho u_i\frac{\partial k}{\partial x_i}=\tau_{ij}\frac{\partial u_i}{\partial x_j}-\beta^*\rho\omega k+\frac{\partial}{\partial x_j}\left[\left(\mu+\sigma_k\mu_t\right)\frac{\partial k}{\partial x_j}\right] \tag{1}$$

$$\rho\frac{\partial \omega}{\partial t}+\rho u_i\frac{\partial \omega}{\partial x_i}=\frac{\gamma}{\nu_t}\tau_{ij}\frac{\partial u_i}{\partial x_j}-\beta\rho\omega^2+\frac{\partial}{\partial x_j}\left[\left(\mu+\sigma_\omega\mu_t\right)\frac{\partial \omega}{\partial x_j}\right]+2\left(1-F_1\right)\rho\sigma_{\omega2}\frac{1}{\omega}\frac{\partial k}{\partial x_j}\frac{\partial \omega}{\partial x_j} \tag{2}$$

Where, K is the turbulent kinetic energy; $u_i(i=1,2,3)$ represents the velocity component on the coordinate axis x_i; μ is the coefficient of kinematic viscosity; μ_t is the coefficient of eddy viscosity; ω is specific dissipation rate; $\beta^*=0.09$; $\sigma_k=0.09$; $\gamma=5/9$;$\beta=0.07$; $\sigma_\omega=2$; $\sigma_{\omega2}=0.44$; the eddy viscosity μ_t is defined as follows:

$$\mu_t=\frac{\rho a_1 k}{\max\left(a_1\omega, SF_2\right)} \tag{3}$$

Where, F_1 and F_2 are the mixed functions to select the *k-ω* model or *k-ε* model for the computational domain.

Mixed function

$$F_1=\tanh\left(\left(\min\left[\max\left(\frac{k^{1/2}}{\beta^*\omega y},\frac{500\nu}{y^2\omega}\right),\frac{4\sigma_{\omega2}k}{CD_{k\omega}y^2}\right]\right)^4\right) \tag{4}$$

$$CD_{k\omega}=\frac{2\sigma_{\omega2}}{\omega}\frac{\partial k}{\partial x_j}\frac{\partial \omega}{\partial x_j} \tag{5}$$

2.2 Computation of the flow field wall area

The wall is the main source of vortexes and turbulences, which has a great impact on turbulences. Therefore, the near wall model affects the accuracy of the fluid numerical solution. In the near wall area, the flow in the boundary layer plays a main role in the entropy increase of the fluid, the viscous damping reduces the tangential velocity fluctuation, and the motor block reduces the normal velocity fluctuation. Outside the near wall area, the increase of the fluid velocity gradient causes the increase in the turbulent kinetic energy, and further leads to the gradual increase in the turbulence of the fluid.

By studying the Nikuradse rough tube test data, Cebeci and Bradshaw defined roughness regimes: hydraulically smooth ($h^+\leq2.25$), transitional roughness ($2.25<h^+\leq90$) and fully rough ($h^+>90$) regimes.

The near-wall logarithmic velocity distribution is as follows:

$$u^+=\frac{1}{\kappa}\ln\left(Ey^+\right)-\Delta B \tag{6}$$

Where, κ is the Karman constant, E is the empirical constant and ΔB is the near-wall logarithmic velocity variation expressed in the dimensionless roughness quantity.

$$\Delta B=0 \quad h^+\leq2.25 \tag{7}$$

$$\Delta B=\frac{1}{\kappa}\ln\left(\frac{h^+-2.25}{87.75}+C_s h^+\right)\times\sin[0.4258(\ln h^+-0.811)$$

$$2.25<h^+\leq90 \tag{8}$$

$$\Delta B=\frac{1}{\kappa}\ln\left(1+C_s h^+\right) \quad h^+>90 \tag{9}$$

$$h^+=\rho h_s u_\tau/\mu \tag{10}$$

Where, C_S is the roughness constant, whose value is related to the roughness type. In this paper, $C_S=0.5$.

2.3 Geometric modeling and meshing

The structural parameters are as follows: blade z=7; impeller diameter = 118mm; the volute is of the involute form; the minimum gap between the shell at the volute tongue and the impeller is 0.5mm; and the minimum spacing between the pressure-bearing surface of the shell and the impeller is 1mm.

According to the requirements of the physical model adopted in the pump CFD analysis, the flow region of the pump is divided into the dynamic region containing the impeller and the lateral static region, as shown in Fig.1. In the splitting process of the model, the locations of the two split surfaces are the key. In principle, they should be so located as to ensure the geometric models of the two regions can generate high-quality meshes without intercrosses.

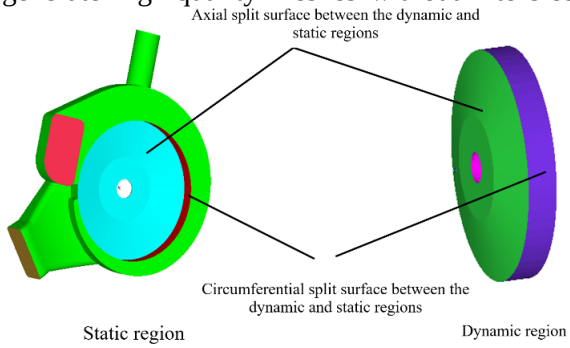

Figure 1. Division of flow regions

In this paper, we use ICEM CFD software to mesh the two parts of the pump computation model and adopt the unstructured tetrahedral mesh. In order to make the physical quantities more accurately exchange between the dynamic and static regions in the solving process, the mesh scale of the interfaces between the two regions should be consistent. At the same time, in order to obtain a better solution convergence, we stretch out a section of volume mesh in the form of triangular prism at the large circulation inlet and outlet of the water pump, respectively. We then carry out mesh-independent calculation and set a total of five kinds of mesh schemes (see Table 1). When mesh count is more than 1.77 million, the calculation result does not change little. The mesh model is shown in Figure 2.

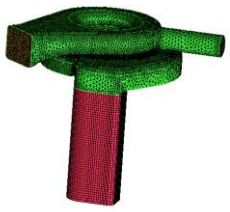

Figure 2. Mesh model for the centrifugal pump

Table 1. Mesh setup scheme

Scheme	Mesh count (10,000)	Computed lift H/m
1	136	16.11
2	154	18.09
3	177	18.12
4	199	18.18
5	221	18.17

2.4 Boundary conditions

The flow of the coolant in the water pump is regarded as a steady, adiabatic and incompressible turbulence; the internal face of the water pump is regarded as hydraulically smooth; the uncoupled implicit algorithm is used, with second order accuracy; the physical parameters of the coolant are selected according to the test; mass flow inlet and outlet; the information transfer between dynamic and static components is achieved by the GGI method.

2.5 Realization approaches for computation

We use the FLUENT software. For turbulence models, we select the standard κ-ε turbulence model and the standard wall equation. In the rotating region, first we select the MRF model to carry out the simulation and compares it with the experimental result. Then we use the SMM model to carry out the simulation, and compare it with the experimental result, and finds out about the effects of model selection for the rotating area on the accuracy of the computation results.

3 COMPUTATION RESULTS AND ANALYSIS

3.1 MRF computation results and analysis

In this paper, we simulate the vehicle centrifugal pump. For the rotating area, we adopt the MRF model. Together we simulate five operating conditions and calculate the lift and efficiency of the centrifugal pump under these operating conditions. The results are shown in Table 2. We compare the results obtained from the CFD

analysis of the pump performance with the experimental data.

By comparing the data shown in the above table, we can see: when the pump rotating speed is higher than 2500rmp, the pump lift calculated by the MRF model is higher than the test value. This is because the default setup of the software takes the wall as smooth, but actually it is rough. As a result, the calculated result is higher; when the rotating speed of the pump is no higher than 2000rpm, the calculated lift is lower than the test value, and the difference between them is quite big. The reason for this is that: when the rotating speed is low, the flow on the interface between the rotating and static regions of the pump can no longer be regarded as homogeneous (not time-varying), which does not meet the prerequisite for using the MRF model for simulation. In this case, a more accurate SMM (Sliding Mesh Model) model is needed, which uses the transient solution method and considers in detail the interaction between the two regions, but this method requires much more computation time and amount than the MRF model.

Table 2. Comparison between CFD computation and test results in the MRF model

No.	Working condition of the water pump		Lift [m]			Efficiency [%]		Determination of the computation result
	Rotating speed [rpm]	Flow [L/min]	Test data	CFD analysis result	Result error	Test	Computation	
1	3400	300	19.11	19.52	2.14	31.06	33.24	Correct
2	3370	300	17.875	18	0.7	31	33.60	Correct
3	2500	240	10.506	10.83	3.1	35.33	35.88	Correct
4	2000	150	7.75	6.28	18.9	35.5	29.26	Incorrect
5	1500	100	5.025	3.4	32.3	#	#	Incorrect
6	1000	50	3	1.55	48.3	#	#	Incorrect

We simulate and analyze the centrifugal pump model under different operating conditions. Fig.3 shows the velocity distribution on the impeller surface simulated through CFD analysis. Fig.4 shows the total pressure distribution on the pump surface simulated through CFD analysis. Fig.5 shows the static pressure distribution on the section in the rotating area of the pump impeller. The cross-section is 10.12mm from the front cover. It can be seen from the three graphs that: the flow velocity at the vortex tongue is relatively high; under the action of the impeller, the fluid movement from the pump inlet changes from being axial to radial, and as the flow channel at the inlet of the impeller shrinks, the flow field at the turning is not uniform and causes a relatively large pressure loss; along the rotation direction of the impeller, the pressure in the flow area between the impeller and the shell is gradually increasing.

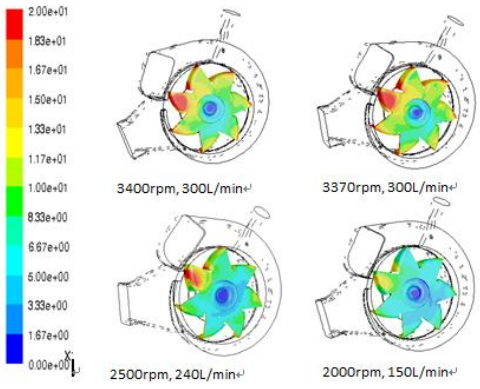

Figure 3. Velocity distribution on the impeller surface under different operating conditions

Figure 3. Velocity distribution on the impeller surface under different operating conditions

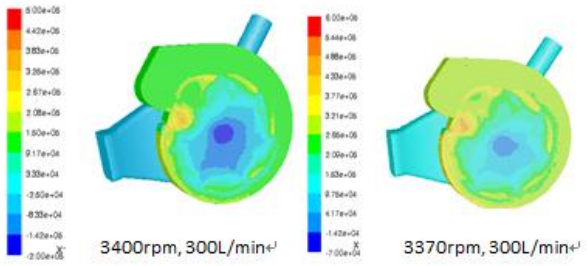

Figure 4. Total pressure distribution on the pump surface under different operating conditions

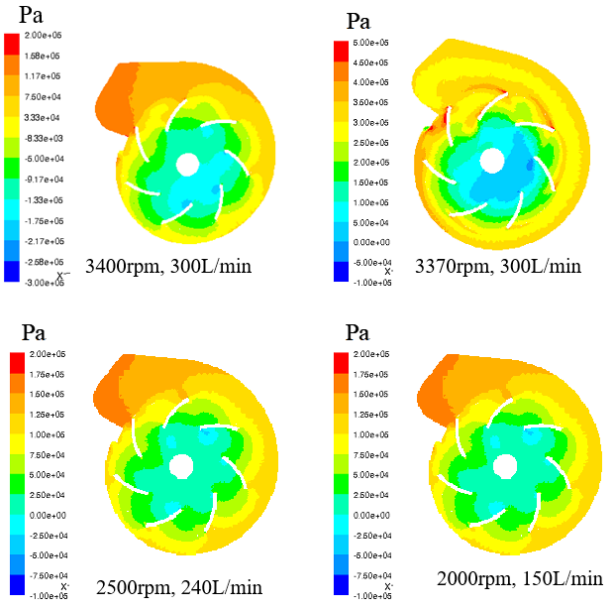

Figure.5. Static pressure distribution on the cross section of the rotating area of the water pump under different working conditions

3.2 SMM model computation results and analysis

The SMM model is set up in the same way as the MRF model, except that the model is changed in the rotating area. Through previous analysis of the simulation result of the flow field in the pump given by the MRF model, we know that the SMM model should be used for simulation when the rotating speed of the pump is low to more accurately reflect the interaction between the rotating and static regions in the pump.

When the SMM model is used, the basic process is as follows: (1) first, we use the MRF model to solve the whole computational domain at steady state, for the purpose of obtaining a steady initial field; (2) we then adjust the setup of the computational domain, including changing the computation model for the rotating fluid region from MRF to SMM, changing the solution method from the original steady state to the transient state, adjusting the relaxation factor of the physical quantity in the control equation accordingly, and setting reasonable time step for the solution (to

ensure that the distance turned in each time step is less than a mesh on the interface).

Taking the working conditions 1500rpm and 100L/min as an example, we use the SMM model for simulation and computation at a time step of 5e-6s. The final calculation result is considered acceptable only after the impeller of the pump rotates for a while from the initial position and the pump lift is substantially constant or fluctuates regularly in a very small range. In this example, after the pump rotates for 2.75 cycles relative to the initial position, the calculation result is basically stable (the monitored outlet pressure shows regular fluctuations in a small range).

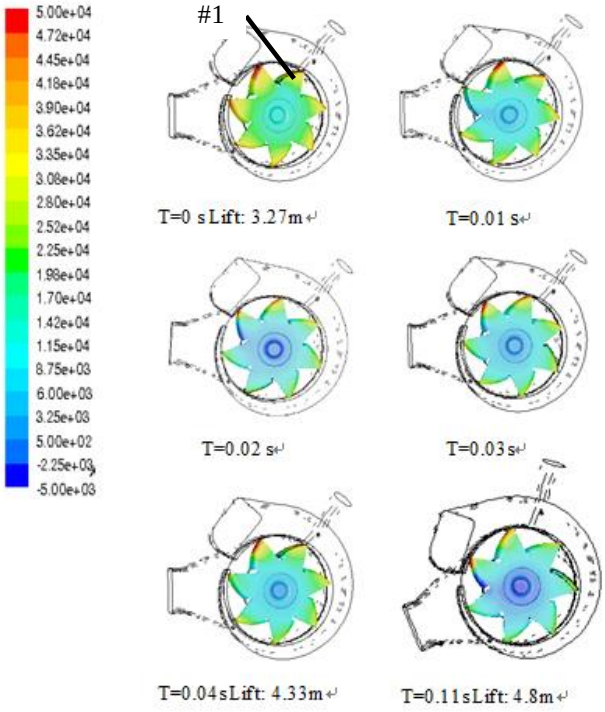

Figure 6. Static pressure distribution on the impeller surface at different time

Fig.6 shows the static pressure distribution of the impeller surface at different time. Fig.7 shows the static pressure distribution on the section of the rotating area where the pump impeller is located at different times, where the cross-section is 10.12mm from the front cover. The result at T=0s is the result obtained from the steady-state simulation by the MRF model. In the figure, the position of the 1# impeller is used as a reference. It can be seen from these two graphs that as the impeller rotates, the static pressure distribution on the impeller surface and the cross section of the pump changes over time. At t=0.11s (the pump turns for 2.75 cycles), the lift of the pump has been increased from 3.27m at the initial time to 4.8m, which is close to the 5.025m measured in the pump bench test. This shows that the state of the water pump simulated by the SMM model under low-speed condition is very close to the actual working state, indicating that this model can be used to predict the performance of water pumps in the design stage.

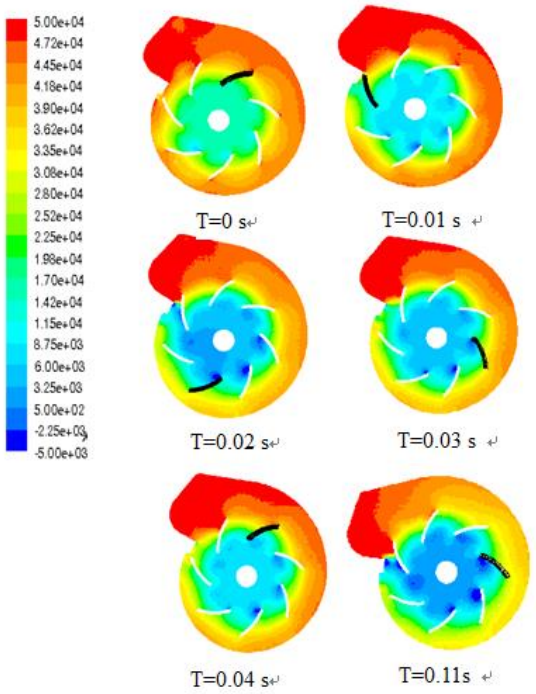

Figure 7. Static pressure distribution on the cross section of the rotating area of the water pump at different time

4 CONCLUSIONS

This paper uses the FLUENT software to carry out simulation computation of the internal flow field of a vehicle cooling centrifugal pump and finds that different models selected for the rotating area lead to different computation results under each working condition and sometimes lead to invalid ones with poor computation accuracy. Under one working condition, different models would also lead to very different computation results. This paper analyzes the causes for such differences and based on the computation processes, obtains the following conclusions:

For the MRF model: when the rotating speed is high, the computed result is consistent with the test one and thus proves to be valid, but that when the rotating speed is no higher than 2000rpm, the computed result is obviously less than the test result. Under the conditions of 3370rpm and 300L/min, the difference between the computed result and the test one is 0.7%; under the conditions of 2500rpm and 240L/min, the difference is 3%, indicating that the computed result is in good agreement with the test one. But under the conditions of 2000rpm and 150

L/min, the computed result is lower than the test one by 18.9% and under the conditions of 1500 rpm and 100L/min, it is lower by 32.3%, which are obviously incorrect.

For the SMM model: considering the inaccurate computation result of the internal flow field of the centrifugal pump given by the MRF model under a low rotating speed, the SMM model is selected for the computation of the rotating area in the centrifugal pump and the lift and efficiency under the conditions of 1500rpm and 100L/min are calculated. After one working cycle of the impeller, the lift is up to 4.8m. Through comparison with the test result, it is found the computation error is 4.4%, and that the computed efficiency is 36.75% and that the test result is 35.8%. Therefore, the computed result is considered valid. However, due to the different computation processes, it takes the SMM model a long time to do the computation. This paper uses a computer with 24 CPU cores and 32G RAM and it takes it 80 hours to the do the computation.

This paper analyzes the cause for the inaccurate computed result in the rotating area of the MRF model under a low rotating speed and finds that the MRF model assumes the flow on the interface between the rotating and the stationary areas of the pump does not vary over time, which is feasible and valid when the impeller is rotating at a high speed. However, when the rotating speed is low, the interface in the computed area needs to be solved by a transient solution, and thus the SMM model should be used to compute the rotating area. When the rotating speed is high, the SMM model can also be adopted, but it costs much more computation amount and time than the MRF model, so when the rotating speed is high, the MRF model is preferred and its computed result meets the requirement.

5 REFERENCES

►Deglon, D., Meyer, C.J. (2006). CFD modeling of stirred tanks:num erical cons iderations. Minerals Eng, 19(10): 1059-1068.

►Franco, M., Zhang, J.F., Gerard, B. (2015). Simulation of a centrifugal pump by using the harmonic balance method. International Journal of Rotating Machinery, 12(1): 1-14.

►Grapsas, A., John, S. (2010). Flow measurements and simulation in a model centrifugal pump impeller. International Journal of Fluid Mechanics Research, 37(2): 149-161

►Jafarzadeh, H., Alishahi, M.M. (2011). The flow simulation of a low-specific-speed high-speed centrifugal pump. Applied Mathematical Modelling, 35(1): 242-249

►Jiang, X., Zhang, L. (2017). Research on the effect of rotation and curvature on turbulence model and their application. International Journal of Heat and Technology, 35(1): 167-176.

►Lin, G.W., Wang, X.L. (21016). Multi-objective optimal scheduling method for power system based on wind power accommodation. Modelling, Measurement and Control A, 89(1): 244-258.

►Liu, L.L., Sun, Z.C., Wan, C.L., Wu, J.M. (2015). Jet flow field calculation & mechanism analysis on hot-air drying oven based on RNG k-ε model. International Journal of Heat and Technology, 33(1): 77-82.

►Muench, C., Ausoni. P., Braun, O. (2010). Fluid-structure coupling for an oscillating hydrofoil. Journal of Fluids and Structures, 26: 1018-1033

►Mukhopadhyay, N., Mondal, M. (2016). Optimization of convective heat transfer model of cold storage with circular fins evaporator using Taguchi S/N ratio and ANOVA. Modelling, Measurement and Control B, 85(1): 79-90.

►Nishino, T., Roberts, G.T., Zhang, X. (2008) Unsteady RANS and detached-eddy simulations of flow around a circular cylinder in ground effect. Journal of Fluids and Structures, 24: 18-33.

►Rabczuk, T., Gracie, R., Song, J.H. (2010). Immersed particle method for fluid-structure interaction. International Journal for Numerical Methods in Engineering, 81: 48-61.

►Rafiee, S.E., Sadeghiazad, M.M. (2016). Three-dimensional CFD simulation of fluid flow inside a vortex tube on basis of an experimental model-the optimization of vortex chamber radius. International Journal of Heat and Technology, 34(2): 236-244.

►Spalart, P.R. (2000). Strategies for turbulence modeling and simulations. International Journal of Heat and Fluid Flow, 21(3): 252-263.

►Yang, Z.G., Bozeman, J., Shen, F.Z. (2002). CFRM concept for vehicle therm al system. SAE Technical Paper Series, 1(1), 207-216.

►Zhang, M., Li, S.B. (2013). Based on Sliding Gird to Calculate the Hydrodynamic Performance of Propeller. Ship Ocean Engineering, 42(5):25-29.

6 NOTATIONS

$CD_{k\omega}$= positive portion of the cross-diffusion in ω-transport equation
R_i= Richardson number
u_τ=frition velocity
y^+= nondimensional distance from the surface
β^*, γ, β= turbulence-model coefficients
k= kinetic energy of turbulence
σ_K, σ_ω=turbulence-model coefficients